Tissue Engineering and Delivery Systems **Biotechnology and Bioengineering**
DOI 10.1002/bit.25493

3D Bioprinting of Biomimetic Aortic Vascular Constructs with Self-Supporting Cells†

Can Kucukgul[1], S. Burce Ozler[1], Ilyas Inci[2], Ezgi Karakas[2], Ster Irmak[2], Devrim Gozuacik[2], Alpay Taralp[3] and Bahattin Koc [1,*]

[1]Industrial and Manufacturing System Engineering, Faculty of Engineering and Natural Sciences, Sabanci University, Istanbul 34956, Turkey

[2]Biological Sciences & Bioengineering, Faculty of Engineering and Natural Sciences, Sabanci University, Istanbul 34956, Turkey

[3]Material Science and Engineering, Faculty of Engineering and Natural Sciences, Sabanci University, Istanbul 34956, Turkey

∗Corresponding author at: Sabanci University, FENS G013, Orhanli-Tuzla, Istanbul, 34956, Turkey. Tel.: +902164839557; E-mail address: bahattinkoc@sabanciuniv.edu (B. Koc).

Received July 4, 2014; Revision Received September 29, 2014; Accepted November 3, 2014

ABSTRACT

Cardiovascular diseases are the leading cause of deaths throughout the world. Vascular diseases are mostly treated with autografts and blood vessel transplantations. However, traditional grafting methods have several problems including lack of suitable harvest sites, additional surgical costs for harvesting procedure, pain, infection, lack of donors and even no substitutes at all. Recently, tissue engineering and regenerative medicine approaches are used to regenerate damaged or diseased tissues. Most of the tissue engineering investigations have been based on the cell seeding into scaffolds by providing a suitable environment for cell attachment, proliferation and differentiation. Because of the challenges such as difficulties in seeding cells spatially, rejection and inflammation of biomaterials used, the recent tissue engineering studies focus on scaffold-free techniques. In this paper, the development of novel computer aided algorithms and methods are developed for 3D bioprinting of scaffold-free biomimetic macrovascular structures. Computer model mimicking a real human aorta is generated using imaging techniques and the proposed computational algorithms. An optimized three-dimensional bioprinting path planning are developed with the proposed self-supported model. Mouse embryonic fibroblast (MEF) cell aggregates and support structures (hydrogels) are 3D bioprinted layer-by-layer according to the proposed self-supported method to form an aortic tissue construct.

KEYWORDS: 3D bioprinting; scaffold-free tissue engineering; tissue engineering of macrovascular structures; biomimetic modeling

Introduction

Cardiovascular diseases are the primary reasons of deaths and they rank among the top ten leading causes of morbidity and mortality (Nemeno-Guanzon et al., 2012). Autografts and blood vessel transplantation are found to be the most effective treatments for vascular diseases. However, autografts have limitations such as lack of autografts in donor site or the patient's deficient health condition. Recently, tissue engineering and regenerative medicine research have been developed for regeneration of damaged or diseased vascular tissues.

In earlier tissue engineering strategies, the cells are seeded into synthetic, biological or composite scaffolds. Especially, synthetic-biologic hybrid scaffold with their biochemical and mechanical properties mimicking the native ECM are strong 3D cell culture platforms for cell physiology and tissue printing studies (Tibbitt and Anseth 2009). However, fabrication of a controlled porous structure with the desired internal architecture might be challenging with traditional scaffold fabrication techniques. Despite these difficulties, several researchers have developed methods for design and bioprinting of functionally gradient porous scaffolds with controllable variational pore size and heterogeneous porous architecture (Khoda et al., 2011; Khoda et al., 2013).

Recently, there are a few studies focusing on vascular and valve tissue engineering using 3D printing techniques. In order to mimic complex 3D anatomy and heterogeneity of aortic valve, root wall and tri-leaflets are 3D printed with poly-ethylene-glycol-diacrylate (PEG-DA) hydrogels. Porcine aortic valve interstitial cells (PAVIC) seeded scaffolds maintained near 100% viability over 21 days (Hockaday et al., 2012). Another study demonstrates that encapsulated aortic root sinus smooth muscle cells (SMC) and aortic valve leaflet interstitial cells (VIC) are viable within the bioprinted alginate/gelatin aortic valve hydrogel conduits (Duan et al., 2012). In (Daniela et al., 2013), human mesenchymal stem cells were encapsulated into agarose hydrogels and cell-laden hydrogel was 3D printed submerged in a

hydrophobic high-density fluorocarbon, which mechanically supports the construct and afterwards can be easily removed. Additionally, cell-laden microengineered hydrogel constructs with an embedded network of vascular –like microchannels were sequentially assembled in a biphasic reactor in order to achieve 3D tubular constructs (Du et al., 2011).

Although there are few studies relevant to the vascular tissue engineering, these approaches are based on scaffold or cell-laden hydrogel based which limit the construction of an entirely biomimetic and biological blood vessels (Norotte et al., 2009). In addition, chronic inflammation, thrombosis and rejection after *in-vivo* implantation could be unpredictable side effects due to the degradation of the materials and the cell-material interaction (Nemeno-Guanzon et al., 2012). Recently, there have been a few research focusing on scaffold-free tissue engineering of small-diameter, multi-layered, tubular vascular and nerve grafts (Marga et al., 2012). A platform-assisted 3D inkjet bioprinting system was utilized in order to fabricate NIH 3T3 mouse fibroblast-based tubes with an overhang structure having a post-printing cell viability above 82% (Xu et al., 2012). Microvascular units consisting of cylindrical or spherical multicellular aggregates are fabricated by the parenchymal and endothelial cells. Afterwards, microvascular units are located in the macrovascular network for the perfusion supporting self-assembly and the connection to the existing network (Jakab et al., 2010). However, the formation of large amounts of spherical or cylindrical aggregates requires a lot of manual work and the fusion process of the spheroids is completed in 5-7 days.

In this paper, 3D bioprinting of a macro-vascular tissue such as aorta directly from medical images is proposed. A computer model of a macro-vascular tissue is generated by biomimicking a real human aorta model directly from medical images. To support the bioprinted mechanically-weak live cell aggregates, a novel self-supporting methodology is

developed. The computer aided algorithms are developed to bioprint self-supporting cell aggregates in 3D for fully biological and scaffold-free macro-vascular tissue engineering.

Materials and Methods

3D Bioprinting System and Hydrogel Preparation

The cells and support biomaterials are 3D printed using Novogen MMX Bioprinter. The 3D bioprinter can print hydrogel biomaterials as well as cylindrical cell aggregates with its two deposition heads equipped with 500 μm diameter sized glass capillaries as shown in **Error! Reference source not found.**. While it is possible to control the printer with its own software for simple geometries, novel path planning strategies for both cell and support material must be developed for complex geometries. The 3D bioprinter can then be controlled directly by the generated scripts and it can print cell aggregates and support hydrogels layer by layer to form the designed tissue structure.

A bio-inert, thermo-responsive hydrogel called NovoGel was used as a support material for 3D printing of the developed models. The preparation of 2% (w/v) NovoGel (Organovo) was carried out with phosphate buffered saline (PBS: Thermo Scientific Hyclone 1X) with Ca^{2+} and Mg^{2+} salts. The solution was mixed with magnetic stirrer and it was kept in microwave for 1 minute on high power settings. Then, the solution was located in a water bath set at 70°C. NovoGel solution was autoclaved following standard liquid sterilization procedures (Kucukgul et al., 2013).

Cell Culture and Staining

Early passage primary mouse embryonic fibroblast (MEFs isolated from C57BL/6 strain) cells were immortalized using SV40 Large T genome using standard protocols. Cells were

cultured at 37 ^{o}C and under 5% CO_2 using DMEM culture medium (Sigma, Germany) supplemented with 10% FBS (Biochrom KG, Germany), 1% Penicillin-Streptomycin (Biological Industries, Israel), 1% L-glutamin (Biological Industries, Israel), 55 μM β-mercaptoethanol (Sigma, Germany) and 0.8 μg/ml puromycin (Sigma, Germany). Subconfluent and low passage cultures were used for this study.

Bio-ink Preparation

Immortalized MEF cells were cultured in 15 cm-diameter culture dishes. Cells were detached from the culture plate using two different approaches. Cells were either detached using 0.1% trypsin (Biological Industries, Israel) for 10 minutes (Exp1), or 2.5 mM EGTA (ethylene glycol-bis(2-aminoethyl ether)-N,N,N´,N) (Idranal VI, Fluka, Germany) in PBS. Following detachment, trypsin or EGTA was neutralized using serum containing medium. Following detachment, cells were centrifuged at 200 x g and supernatant was discarded. The cell pellet was resuspended to obtain 10 x 10^6 cells / 20 ml medium incubated at 37°C in 15 ml-conical tubes under rotation (PTR-30 Grant-Bio rotator, U.K). Following pelleting, cells were resuspended in 1 ml medium and transferred into 1.5 ml Eppendorf tubes and centrifuged again (1000 x g). Then, the cell pellets were drawn into capillary tubes. Following incubation, cells inside the capillary tubes were extruded into cylindrical grooves on agarose gel (2% in PBS). Then, plates were covered with culture medium and put into the incubator until cylindrical bioinks are formed. Cylindrical bioink MEF cells were drawn back into capillary tubes and bioprinting was performed using the 3D bio-printer.

For continuous bioprinting, cells were centrifuged at 200 x g. The pellet was resuspended to have 20 x 10^6 cells / 6.5 ml and transferred into 15 ml-conical tubes. Following rotation at 37°C, cells were pelleted and transferred into Eppendorf tubes. Cell pellets in 1.5 ml

Eppendorf tubes (60 x 10^6 cells in total) were transferred into capillaries by continuous bioprinting.

Staining and Western Blotting

To detect cylindrical cell aggregate fusion, Hoechst 33342 (Invitrogen, U.S.A) and Acridine orange (AO) (Invitrogen, U.S.A) staining was used. Immortalized MEF cells stained 15 min. with either Hoechst 33342 (final concentration 1 μg/ml) or AO (final concentration 2 μg/ml) and used for bioink preparation using protocols explained below. Florescent signals were analyzed under an Olympus IX-70 fluorescent microscope (Olympus, Japan).

Cellular stress and viability was analyzed by immunoblotting. Anti-rabbit anti-caspase 3 (Cell Signaling Technology, U.S.A), anti-rabbit anti-LC3B (Sigma-Aldrich, Germany), anti-mouse anti-beta actin (Sigma-Aldrich, Germany), anti-mouse anti-SQSTM1/p62 (Abnova, Taiwan), anti-rabbit anti-procaspase 3 (Pro-Csp-3) (Santa Cruz Biotechnology, U.S.A), anti-rabbit anti-PARP (Cell Signaling Technology, U.S.A) and anti-rabbit anti-cleaved PARP (Cell Signaling Technology, U.S.A) antibodies were used as primary antibodies. Peroxidase conjugated anti-rabbit (Jackson Laboratory, U.S.A) and peroxidase conjugated anti-mouse (Jackson Laboratory, U.S.A) antibodies were used as secondary antibodies. Cylindirical bioinks were transferred into 1.5 ml Eppendorf tubes, centrifuged at 1000 x g for 10 minutes and pellets were lysed in RIPA buffer (50 mM Tris pH 7.4, 150 mM NaCl, 1 % NP40, 0.25 % Na-deoxycholate) supplemented with complete protease inhibitor cocktail (Roche, Germany) and 1 mM phenylmethylsulfonyl fluoride (PMSF). Protein concentration was measured by using BCA protein assay. Protein extracts were separated in 12–15 % SDS-polyacrylamide gels (SDS-PAGE) and then transferred to nitrocellulose membranes (Advantec MFS Inc, Japan) using electroblotting. Membranes were blocked in 5 % non-fat milk in PBS-T (3.2 mM Na2HPO4, 0.5 mM KH2PO4, 1.3 mM KCl, 135 mM NaCl, 0.05 %

Tween 20, pH 7.4) for 1 h. Following incubation with primary antibodies and secondary antibodies, blots were developed on X-ray films (Fuji, Japan) using West-pico chemiluminescence detection reagent (Pierce, Germany).

3D Bioprinting of Aortic Vascular Structure Using Self-Support

A roadmap of the proposed approach is presented in **Error! Reference source not found.**. Firstly, a medical image obtained from computer tomography (CT) or magnetic resonance imaging (MRI) is used to obtain the geometric and topological information of the targeted vascular tissue (Figure 2.a). Secondly, the STL (mesh) model of aorta converted to a parametric smooth surface (Figure 2.b). The computer model is then sliced for the layer-based 3D bioprinting process and the proposed methodology has been implemented in every slice to compute the locations for both cellular aggregates and support structures. To support the bioprinted live cell aggregates, a novel self-supporting methodology is developed (Figure 2.c). The generated cell and support 3D printing paths are used to control the bioprinter for 3D printing of a biomimetic aortic construct (Figure 2.d). The details of the proposed methodology are given below.

3D Imaging

To be able to mimic and 3D bioprint a blood vessel, the original geometry of the vessel has to be obtained and transformed in a way that the vessel can be used in computer aided modeling. In this work, the main abdominal aorta model is used to highlight the proposed methods capabilities for 3D bioprinting of macrovascular structures. For segmentation of the aorta from the rest of the internal organs, region growing tools of Mimics software (Mimics, Medical Image Segmentation for Engineering on Anatomy) are used as shown in Figure 2.a. The initial geometric information of the model is then represented as a mesh model or

stereolithography (STL) model as shown in Figure 3.b, which will be used for computer-aided biomodeling methodology described at the following sections.

Biomodeling of Aorta

As shown in Figure 3.a-b, the derived STL model of the aorta is not smooth and represented by numerous triangular facets. A novel biomodeling method is developed to convert these mesh (triangular facets) structures into smooth parametric surfaces to be used for 3D bioprinting.

A marching algorithm is developed to calculate section curves starting from bottom edge curve EC_b until the top edge curve EC_t. The developed algorithm marches the vertices $V = \{v_{i,l}\}_{l=1..L}$ of all the faces $F = \{f_i\}_{i=1..I}$ of the STL model to form the section curves. The set of sections is represented as $S = \{s_m\}_{m=1..M}$, and each section is defined with *n* vertices (points) represented as $S_{m,n} = \{s_{m,n}\}_{n=1..N}$. Furthermore, for each section curve there will be center points $CP = \{cp_m\}_{m=1..M}$ reflecting the area weight-based center points for that section curve, and respective radius values $R = \{r_m\}_{m=1..M}$ reflecting the radius of the maximally-inscribed sphere of that section curve.

The computation of the Cartesian coordinate center point and the respective radius value of the m^{th} section curve with *n* vertices is as follows:

$$S_{m,n} = \{s_{m,n}\}_{n=1..N} \rightarrow \text{A set of } n \text{ points in the } m^{\text{th}} \text{section}$$

$$cp_m = \left(\frac{\sum_{n=1..N} s_{m,n}(x)}{N}, \frac{\sum_{n=1..N} s_{m,n}(y)}{N}, \frac{\sum_{n=1..N} s_{m,n}(z)}{N} \right) \quad (1)$$

$$r_m = \min_{n=1..N} \left(\left\| \overline{s_{m,n}, cp_m} \right\| \right)$$

When the top section is reached by marching through the section curves, the algorithm builds a B-spline curve, which will be the centerline for the parametric surface. Mathematically, this parametric B-spline centerline curve is defined as (Piegl and Tiller 1997):

$$CC(u) = \sum_{i=1}^{m} N_{i,p}(u) \cdot cp_i \qquad 0 \le u \le 1 \quad \text{Where B-spline basis function is;}$$

$$N_{i,0}(u) = \begin{cases} 1 & \text{if } u_i \le u < u_{i+1} \\ 0 & \text{otherwise} \end{cases} \tag{2}$$

$$N_{i,p}(u) = \frac{u - u_i}{u_{i+p} - u_i} N_{i,p-1}(u) + \frac{u_{i+p+1} - u_i}{u_{i+p+1} - u_{i+1}} N_{i+1,p-1}(u)$$

Where cp_i's are the control points, and the $N_{i,p}(u)$ are the pth-degree B-spline basis functions as defined above with the knot vector $U = \{u_0, \ldots, u_m\}$.

Then the parametric B-spline surface of the aorta model is generated using the centerline curve with respect to the average radius value of relevant center points as shown in Figure 3.c. A general form of the swept surface is given by (Piegl and Tiller 1997):

$$S_k(u,v) = CC(u) + M(u)\mathrm{T}(v) \qquad \text{Where } 0 \le u \le 1 \text{ and } 0 \le v \le 1$$

$$T(v) = \left(r_{avg} \cos(v), r_{avg} \sin(v) \right) \tag{3}$$

Where $M(u)$ is a 3x3 matrix incorporating rotation and nonuniform scaling of T(v) as a function of u.

As explained above, generating a smooth aortic model from the mesh model is determined using Algorithm 1.

Algorithm 1. Generating NURBS Surface(s) from Mesh

Input:

M_k: Mesh

$EC = \{EC_{b,t}\}$: two edge curves on Mesh

$F = \{f_i\}_{i=1..I}$: a set of faces on Mesh

$V = \{v_{i,l}\}_{l=1..L}$: a set of vertices on Mesh

Output:

$S_k(u,v)$: generated B-spline Surface(s)

Start

Initialize$i \leftarrow 1$, $m \leftarrow 1$

$S_1 \leftarrow EC_b$

Mark vertices of S_1 as *visited* in set V

$cp_m \leftarrow$ calculate cp_m using Equation(1)

$r_m \leftarrow$ calculate $r_m$using Equation(2)

$m \leftarrow m + 1$

For (m=2 to M){// for all *section* curves

For (i=1 to I) {// for all faces

If ($v_{i,l} + v_{i,l+1} + v_{i,l+2} = 1$// only one vertex of a face $f_i$is *visited*) **Then** {

// determine subsequent*section's* (S_m) points (vertices)

If $v_{i,l} = 0$ **Then** $s_{m,n} \leftarrow v_{i,l}$

If $v_{i,l+1} = 0$ **Then** $s_{m,n+1} \leftarrow v_{i,l+1}$

If $v_{i,l+2} = 0$ **Then** $s_{m,n+2} \leftarrow v_{i,l+2}$

}

}

Mark vertices of the $S_m$curve as *visited* in set V

$cp_m \leftarrow$ calculate cp_m using Equation(1)

$r_m \leftarrow$ calculate $r_m$using Equation(2)

}

$CC(u) \leftarrow$ approximate a centerline curve with the control points using Equation (2)

$S_k(u,v) \leftarrow$ Build the surface along $CC(u)$ with respect to its control point's average radius value using Equation (3)

End

Self-Supporting Model Support Structure Generation for Aorta

Previous works on scaffold-free 3D bioprinting of vascular structures are based generally on simple vertical extrusions (Christopher et al., 2013; Marga et al., 2012). Not only because of its complex geometry, but also due to the dynamic structures of both cells and hydrogels, it is challenging to build such structures in 3D. Here, an anatomically correct 3D bioprinting of vessels is aimed; therefore, mechanically-weak cellular aggregates should be supported in 3D until cell fusion.

After the smooth surface model of aorta $S_k(u,v)$ is generated, an optimum 3D bioprinting topology needs to be determined in order to obtain an anatomically correct representation of the vessel. The path planning for both cellular aggregates and hydrogel support structures is calculated in this section. Both cellular aggregates and support structures are printed by a glass capillary in a gel like form layer by layer to form the 3D tissue construct. Because of the fact that bioprinted materials are not self shape conserving, both cells and support structures should accordingly be placed on the valleys of the preceding layer (shown in Figure 4) in order to provide cell fusion and structure conservation and most importantly, to reach correct anatomical model of the original vessel.

Since the targeted vascular construct is printed layer by layer, the vessel's surface representation is sliced with successive planes which resulted in contour curves

$C_{j,0}(t) = \{c_{j,0}\}_{j=1..totalLayers}$ for each layer, the total number of contour slices equals to *totalLayers*, as shown in Figure 5.a and calculated by Equation (4).

$$totalLayers = \frac{ModelHeight}{d_{capillary}} \tag{4}$$

Where *ModelHeight* is the total height of the aorta model and the $d_{capillary}$ is the diameter of the capillary.

The number of cylinders for each layer is then determined by the $maxStep_j$ value using Equation (5)

$$maxStep_j = topSupport + totalLayers - j \tag{5}$$

where *topSupport* is the total number of support cylinders that is specified just for the top-most layer (in this work, *topSupport* variable equals to 4). To conserve the general shape of the vessel on each layer and to prevent the deformation of weak cellular aggregates, each contour curve is offset using the $maxStep_j$ value of the specific layer on xy-plane as shown in Figure 5.a. The initial offset amount $O_{j,i} = \{o_{j,i}\}_{i=1..maxStep_j}$ for a layer can be found by the following formula:

$$o_{j,i} = \left(\left(maxStep_j/2\right) - \left(i-1\right)\right) \times d_{capillary} \tag{6}$$

Where $d_{capillary}$ is diameter of the glass capillary used.

The initial offset amount for a layer is strictly positive, resulting in exterior offset curves. However, offset amount is dropped by the capillary diameter for each successive cylinder on that layer. Therefore, after ($maxStep_j$/2) cylinders, offset amount will become negative resulting in interior offset curves as shown in Figure 5.a. Thus, cellular aggregates are supported from both inner and outer directions. As $c_{j,0}(t)$ defines a contour curve of the surface on a given height and a curve parameter *t*, then the offset curves with respect to the $o_{j,i}$ will be:

$$c_{j,i}(t) = c_{j,0}(t) + o_{j,i}\overrightarrow{N_{j,i}}(t)_{i=1..\max Step_j} \quad \text{Where,} \tag{7}$$

$\overrightarrow{N_{j,i}}(t)$ = unit normal vector on curve $c_{j,0}(t)$ at a parametric location t.

The support structures are printed first, and then the cellular aggregates in order to prevent cell outflow and to preserve anatomically correct shape of the modeled vessel as shown in Figure 5.b.

As can be seen from Equation (4-7), the total number of cylinders at a layer (cellular aggregates + support structures) are increasing by one at each layer through the bottom and calculated based on the geometry of the aorta model. An increase in the number of support cylinders for the top-most layer results in a thicker outer support for the planned model.

The diameters of the support structures at a given layer *j* can be approximated by Equation (8), as layer numbers increase through top, the support diameters tend to converge to the aorta model:

$$\text{Support Diameter}_j = (totalLayers + topSupport - j) \times d_{capillary} + \text{contour's diameter}_j \tag{8}$$

Where contour's diameter is the approximation of the diameter of the model's contour at layer *j*. Since the developed algorithm uses the model directly from medical images, the generated contours aren't necessarily circular in shape.

After appropriate sections of the cell composition and support structure are determined for each layer, the tool path planning for cell-biomaterial topology is calculated. Then, layer by layer, these cylindrical aggregates of the cell and gels will be printed accordingly a file that is generated by Algorithm 2 using a 3D bioprinter.

Algorithm 2. Self-Supporting Model Support Structure Generation

Input:

$S_k(u,v)$: generated NURBS Surface

$d_{capillary}$: diameter of the glass capillaries

Output:

Finalized vascular model, with support structure

Path planning for 3D-Bioprinting (a compatible script file for the 3D-Bioprinter)

Start

Initialize $totalLayers \leftarrow (surfaceHeight/d_{capillary})+1$, $j \leftarrow 1$, $n \leftarrow 1$, $i \leftarrow 1$, $contourLevel \leftarrow 0$

Initialize $maxStep_j \leftarrow topSupport+totalLayers-j$

For (j = 1 to $totalLayers$) {

$contourLevel \leftarrow contourLevel + d_{capillary}$

If ($c_{j,0} \leftarrow$ contouring the surface from a given *contourLevel*, results in a closed curve) **Then** {

Initialize $o_{j,i} \leftarrow (maxStep_i/2) \times d_{capillary}$

For (i = 1 to $maxStep_i$) {

$c_{j,i} \leftarrow$ offset $c_{j,0}$ by $o_{j,i}$using Equation (7)

Initialize $curveLength \leftarrow$ length($c_{j,i}$)

If ($curveLength < minSegmentLength$) **Then** {**Exit For**} // to prevent self intersection in offset operations

If ($i = maxStep_i/2$ or $i = maxStep_i/2+1$) **Then** {

Store $c_{j,i}$ and *curveLength* in the script file as cellular structure}

Else{Store $c_{j,i}$ and *curveLength* in the script file as support structure}

$o_{j,i} \leftarrow$calculate $o_{j,i}$using Equation (6)

}

$maxStep_j \leftarrow topSupport + totalLayers - j$ }

}

End

Results & Discussion

Implementation of the Self-Supporting Model

Rhinoscript language is used for implementation of the presented algorithms. However, the algorithms can also be implemented by variety of different programming languages. Therefore, the developed algorithms are fully portable. The initial geometry is obtained by using Mimics software and its sample human aorta MRI data. Because of the 3D printer capillary size, the original MR data is scaled down by almost 50%. The whole aorta surface model, which is extracted from the STL file by Algorithm 1, is 50 mm high and its diameter is around 9 mm. For the illustration of the proposed method, a partial aorta model with 3.5 mm height is extracted with Algorithm 1 and its path planning for 3D bioprinting is obtained by Algorithm 2. As illustrated in Figure 2.c, by the cross sectional view, blue cylinders are representing support structures, where red ones represent fibroblast cells.

MEF cell aggregates and support structures are 3D printed layer-by-layer according to the developed Self-Supporting method. As shown in Figure 6, the MEF cells are successfully printed at the valleys formed by the support material (hydrogel).

The bioprinter's deposition speed for support structures and cellular aggregates is set 3 mm/s and 2 mm/s respectively. The optimum speeds are determined after various bioprinting trials. The bioprinter can only aspirate 65 mm hydrogel/cell aggregates into its capillaries, therefore the total printing time is effected by this limitation. Printing a 65 mm piece of material approximately takes about 1 minute, for both cellular aggregates and support structures, including aspiration and chilling times. The bioprinting path for the aorta model shown in Figure 2 consists of 85 support material pieces (12 layers, as shown with blue cylinders in Figure 2.c) and 16 cellular aggregate pieces (for 8 layers, as shown with red cylinders in Figure 2.c). The total printing time for the model was approximately 100 minutes.

In order to compare the final printed structure against the designed structure, a picture of the 4th layer was taken during the printing process as shown in Figure 7. Several different arbitrary points were marked on the taken picture (red points in Figure 7) in order determine the distance between the middle point (blue circle in Figure 7) and cell/gel stripe boundaries using ImageJ software. Three random points (1-2-3) are taken from the outer support material boundary, three points (4-5-6) are taken from the outer cellular aggregate boundary, and the next three points (7-8-9) are taken from the intersection border of the fifth and sixth support material cylinder, and the last three points (10-11-12) are taken from the inner cellular aggregate boundary of the 4th layer. The picture of the printed structure and the designed model are overlapped so that the same distances are measured on the model according to the marked points and shown in Table 1.

The accuracy of the printed cellular aggregates changes between 91% - 95%, while it is around 97% for support structures. The reason of reaching a higher accuracy in support structures relies on that the fact that the hydrogel material is mechanically stronger than the cellular aggregates. Additionally, overall cumulative errors of the support structure may affect the accuracy of the cellular aggregates adversely.

Bioink analysis and optimization

Programmed cell death and cellular stress responses are important issues to face with when dealing with cells grown outside their natural environments (Gozuacik and Kimchi 2004; Gozuacik and Kimchi 2007). A major stress mechanism activated during conditions faced by cells during tissue engineering studies is macroautophagy (Autophagy herein).

Initially, the bioink was prepared using cylindrical cell aggregates method (see the Materials and Methods section). We tested whether incubation of the bioink (20, 40 or 80 min.) within

the capillaries would result in cellular stress and death sensitization. As shown in Figure 8.a, the stripe printing protocol led to the activation of autophagic stress responses as shown by LC3-I to LC3-II conversion and p62 degradation. Moreover, apoptotic cell death was activated under this conditions and the amplitude was proportional to incubation time: Caspase-3 activation and PARP cleavage were observed starting from 20 min. of incubation and reaching a maximum at 80 min (Figure 8.a). Cell cylinders printed under these conditions were followed for 4 days. Although immediately after printing bioink cylinders looked compact and healthy, following 1 day incubation, the cell cylinders started to dissolve, most probably, as a result of the death of some of the cells that make up the cell cylinders (Figure 8.b).

Encouragingly, printed cylindrical cell aggregates stained using two different color dyes were able to fuse under our experimental conditions (Figure 9.a). To improve the printing protocol and minimize the stress imposed on the cells of the bioink, we omitted the capillary incubation and manipulation steps. We switched to the continuous bioprinting protocol design details of which was explained above. This new approach also allowed us to obtain longer cell cylinders and made printing possible in multiple layers and in complicated forms. Using the continuous bioprinting, we were able to design and 3D print MEF bioink cylinders corresponding to the size and shape of a complete human aorta ring (Figure 9.b). To check whether apoptotic death mechanisms were activated in cells making-up the ring, proteins were extracted and immunoblots were performed. Although caspase-3 activation could be seen in control extracts of the same cell type treated with a death inducer, there was no activation in continuously printed bioink ring cells (Figure 9.c). Therefore, there was no apoptotic cell death activation in continuously printed bioink cells, allowing cell fusion and robust ring formation.

Conclusion

In this study, novel computer aided algorithms are developed in order to 3D bioprint hybrid cell and biomaterial scaffold-free macro-vascular structures. The tool path design and 3D printing parameters are optimized for a well-formed 3D printing. After the segmentation of a part of aorta with imaging and segmentation software, the attained geometry of the aorta was converted to CAD model. In order to develop path planning and optimization, parametric surfaces are generated from mesh. For 3D bioprinting of cylindrical cell aggregates according to the aorta model, a self-supporting structure is developed with computational algorithms. Support structure and MEF cells are successfully printed with the Self-Supporting methodology. A CAD software package, Rhino3D using Rhinoscript language, was used for the implementation of all methodologies. The outputs of the developed algorithms are instruction for the Novogen MMX 3D Bioprinter. The modeled part of the aortic tissue structure was successfully 3D bioprinted.

The proposed bioprinting strategies increase the contact of cylindrical cellular aggregates in adjacent bioprinted layers and facilitate the fusion of cells. However, the amount of support structures and therefore the printing time increase depending on the size of the modeled structure. Since the 3D bioprinter is equipped with 75 and 85 mm long capillaries for cell aggregates and support material respectively, the maximum length of material that can be extruded each time is limited. Therefore, the capillary is loaded with support structure or cell aggregates each time during the printing process which slows down the process and prevents a full-continuous printing. Even the proposed bioprinting strategies enable the use of the maximum capillary volume for each extrusion and therefore provide a semi-continuous bioprinting process, it is still challenging to create large structures.

Although the 3D bioprinter is placed in a biosafety cabinet to ensure the sterile conditions, a large cell construct may not survive a long printing process and the cell viability may

decrease with time. In order to keep the printed cells alive, a small amount of culture medium is dispensed on the top of the printed cellular aggregate to prevent the dehydration. As mentioned above, the tissue construct is bioprinted on a flat mold prepared with 2% agarose solution. The mold could dry and deform based on the humidity of the environment and therefore should also be hydrated during the printing process.

The bioprinting system has been used to print various types of cells including human/mouse smooth muscle, endothelial and fibroblast cells. However, obtaining sufficient amount of cells using general cell culture protocols can take a long time based on the cell type. Therefore, the cell types affect the bioink preparation time before the printing process.

To optimize the bioink preparation, autophagy analyses were performed during bioink preparation and after the printing of aortic structure. The results showed that the cell aggregates were printed without any apoptotic cell death activation allowing cell fusion and robust tissue formation.

Acknowledgement

This research is supported by The Scientific and Technological Research Council of Turkey (TUBITAK) grant number 112M094, EU FP7-PEOPLE-2011-CIG awarded to Dr. Koc and the Sabanci University Internal Grant.

References

Christopher MO, Francoise M, Gabor F, Cheryl MH. 2013. Biofabrication and testing of a fully cellular nerve graft. Biofabrication 5(4):045007.

Daniela FDC, Andreas B, Michael W, Jörg J, Sabine N, Wilhelm J-D, Horst F. 2013. Three-dimensional printing of stem cell-laden hydrogels submerged in a hydrophobic high-density fluid. Biofabrication 5(1):015003.

Du Y, Ghodousi M, Qi H, Haas N, Xiao W, Khademhosseini A. 2011. Sequential assembly of cell-laden hydrogel constructs to engineer vascular-like microchannels. Biotechnology and Bioengineering 108(7):1693-1703.

Duan B, Hockaday LA, Kang KH, Butcher JT. 2012. 3D Bioprinting of heterogeneous aortic valve conduits with alginate/gelatin hydrogels. Journal of Biomedical Materials Research Part A 101A(5):1255-1264.

Eberhart K, Oral O, Gozuacik D. 2014. Chapter 13 - Induction of Autophagic Cell Death by Anticancer Agents. In: Hayat MA, editor. Autophagy: Cancer, Other Pathologies, Inflammation, Immunity, Infection, and Aging. Amsterdam: Academic Press. p 179-202.

Faulkner-Jones A, Greenhough S, King JA, Gardner J, Courtney A, Shu W. 2013. Development of a valve-based cell printer for the formation of human embryonic stem cell spheroid aggregates. Biofabrication 5(1):015013.

Gozuacik D, Kimchi A. 2004. Autophagy as a cell death and tumor suppressor mechanism. Oncogene 23(16):2891-2906.

Gozuacik D, Kimchi A. 2007. Autophagy and cell death. Current Topics in Developmental Biology 78:217-45.

Hockaday LA, Kang KH, Colangelo NW, Cheung PYC, Duan B, Malone E, Wu J, Girardi LN, Bonassar LJ, Lipson H and others. 2012. Rapid 3D printing of anatomically accurate and mechanically heterogeneous aortic valve hydrogel scaffolds. Biofabrication 4(3):035005.

Jakab K, Norotte C, Marga F, Murphy K, Vunjak-Novakovic G, Gabor F. 2010. Tissue engineering by self-assembly and bio-printing of living cells. Biofabrication 2(2):022001.

Khoda AKM, Ozbolat IT, Koc B. 2011. A functionally gradient variational porosity architecture for hollowed scaffolds fabrication. Biofabrication 3(3):034106.

Khoda AKM, Ozbolat IT, Koc B. 2013. Designing heterogeneous porous tissue scaffolds for additive manufacturing processes. Computer-Aided Design 45(12):1507-1523.

Kucukgul C, Ozler B, Karakas HE, Gozuacik D, Koc B. 2013. 3D Hybrid Bioprinting of Macrovascular Structures. Procedia Engineering 59(0):183-192.

Marga F, Jakab K, Khatiwala C, Shepherd B, Dorfman S, Hubbard B, Colbert S, Gabor F. 2012. Toward engineering functional organ modules by additive manufacturing. Biofabrication 4(2):022001.

Nemeno-Guanzon JG, Lee S, Berg JR, Jo YH, Yeo JE, Nam BM, Koh Y-G, Lee JI. 2012. Trends in tissue engineering for blood vessels. J. Biomed. Biotechnol. 2012:14.

Norotte C, Marga FS, Niklason LE, Forgacs G. 2009. Scaffold-free vascular tissue engineering using bioprinting. Biomaterials 30(30):5910-5917.

Piegl L, Tiller W. 1997. The NURBS Book: Springer. 646 p.

Tekirdag K, Ozturk D, Gozuacik D. 2013. Alteration in Autophagic-lysosomal Potential During Aging and Neurological Diseases: The microRNA Perspective. Curr Pathobiol Rep 1(4):247-261.

Tibbitt MW, Anseth KS. 2009. Hydrogels as extracellular matrix mimics for 3D cell culture. Biotechnology and Bioengineering 103(4):655-663.

Xu C, Chai W, Huang Y, Markwald RR. 2012. Scaffold-free inkjet printing of three-dimensional zigzag cellular tubes. Biotechnology and Bioengineering 109(12):3152-3160.

List of Figure Legends

Figure 1. 3D Bioprinter.

Figure 2. Roadmap of the proposed methodology. **(a)** Segmentation of an aorta from abdominal region based on region growing. **(b)** The STL (mesh) model of aorta converted to a parametric smooth surface. **(c)** Representation of the 'Self-Supporting' method, with vessel (grey), cellular aggregates (red) and support structures (blue). (please see the color version) **(d)** 3D printed MEF cellular aggregates.

Figure 3. (a-b) STL file of the aorta, mesh structure. **(b)** The modeled Aorta's edge curves (green & red) and the initial section curve (red). **(b-c)** STL (mesh) surface of aorta, the initial center points & smoothed representation of the centerline curve. Generation of smooth NURBS surface from mesh model (aorta).

Figure 4. Three consecutive example layers showing how support structures (blue) and cellular aggregates (red) are placed on the valleys of the preceding layer.

Figure 5. (a) The slicing process of aorta and the placement of the support structures & cellular aggregates at jth layer. (see the color version) **(b)** The bioprinting topology for three example consecutive layers, of both support structures and cellular aggregates.

Figure 6. 3D printed MEF cell aggregates of originally mimicked aorta in 'Self-Supporting' model.

Figure 7. Comparison of the accuracy between designed and printed structures

Figure 8. Cellular stress and death activation following capillary incubation and stripe printing of the bioink. (a) MEFs were prepared following the stripe printing protocol and incubated 20, 40, 80 min. in glass capillaries prior to printing (capillary) or not (Control).

LC3 lipidation (LC3-I to LC3-II conversion) and p62 degradation were used as autophagic activity markers. Pro-caspase-3 and PARP cleavage were used as markers of apoptosis. β-actin was used as a loading control. (b) Phase contrast microscopy and Hoechst nuclear staining pictures of stripes immediately after printing (Day 0) or following incubation for 1 or 4 days.

Figure 9. Printed stripes could fuse and form biologically relevant aorta ring-like tissue precursors. (a) Fusion of stripes stained with Acridine Orange (Red) or Hoechst (Blue) dyes. (b) Image of multiple layers of MEF bioink that was 3D printed in the shape of a human aorta ring. (c) Analysis of apoptotic cell death in protein extracts obtained from printed aorta rings. Exp1, Experiment 1 and Exp2, Experiment 2 (See Materials and Methods for experiment details). Active caspase-3 immunoblots were performed on the stripes. Cont, positive control mouse embryonic fibroblast cells treated O/N with tunicamycin (1 μg/ml). β-actin, loading control.

Table 1. Measurements of the designed and bioprinted structures

Point Numbers	Designed Structure (mm)	Printed Structure (mm)	Error (%)
1	10.602	10.261	3.22
2	10.637	10.323	2.95
3	10.764	10.473	2.70
4	5.138	5.595	8.89
5	5.164	5.409	4.74
6	5.046	5.301	5.05
7	7.432	7.231	2.70
8	7.724	7.562	2.10
9	7.632	7.45	2.38
10	4.217	3.939	6.59
11	4.139	3.853	6.91
12	4.031	3.819	5.26

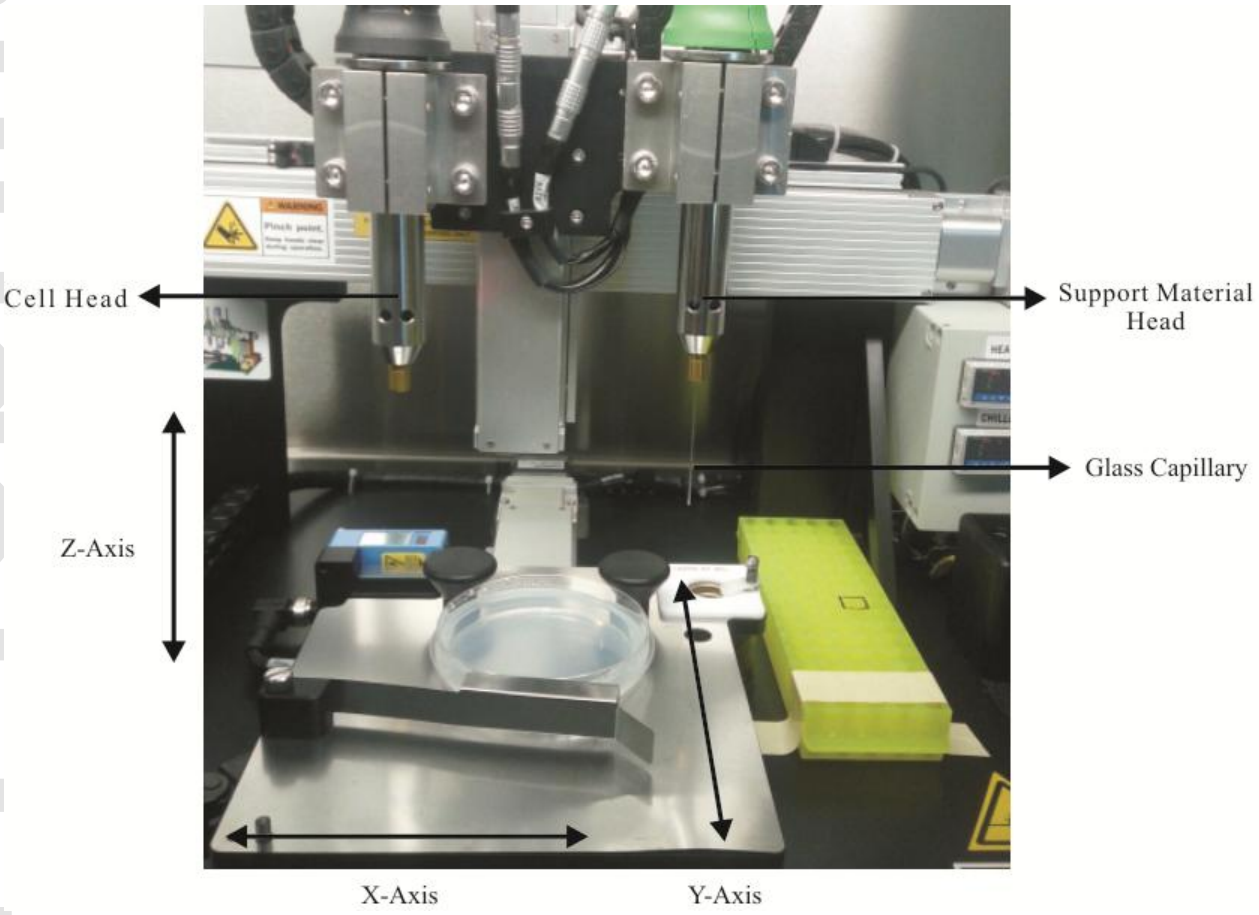

Figure 1

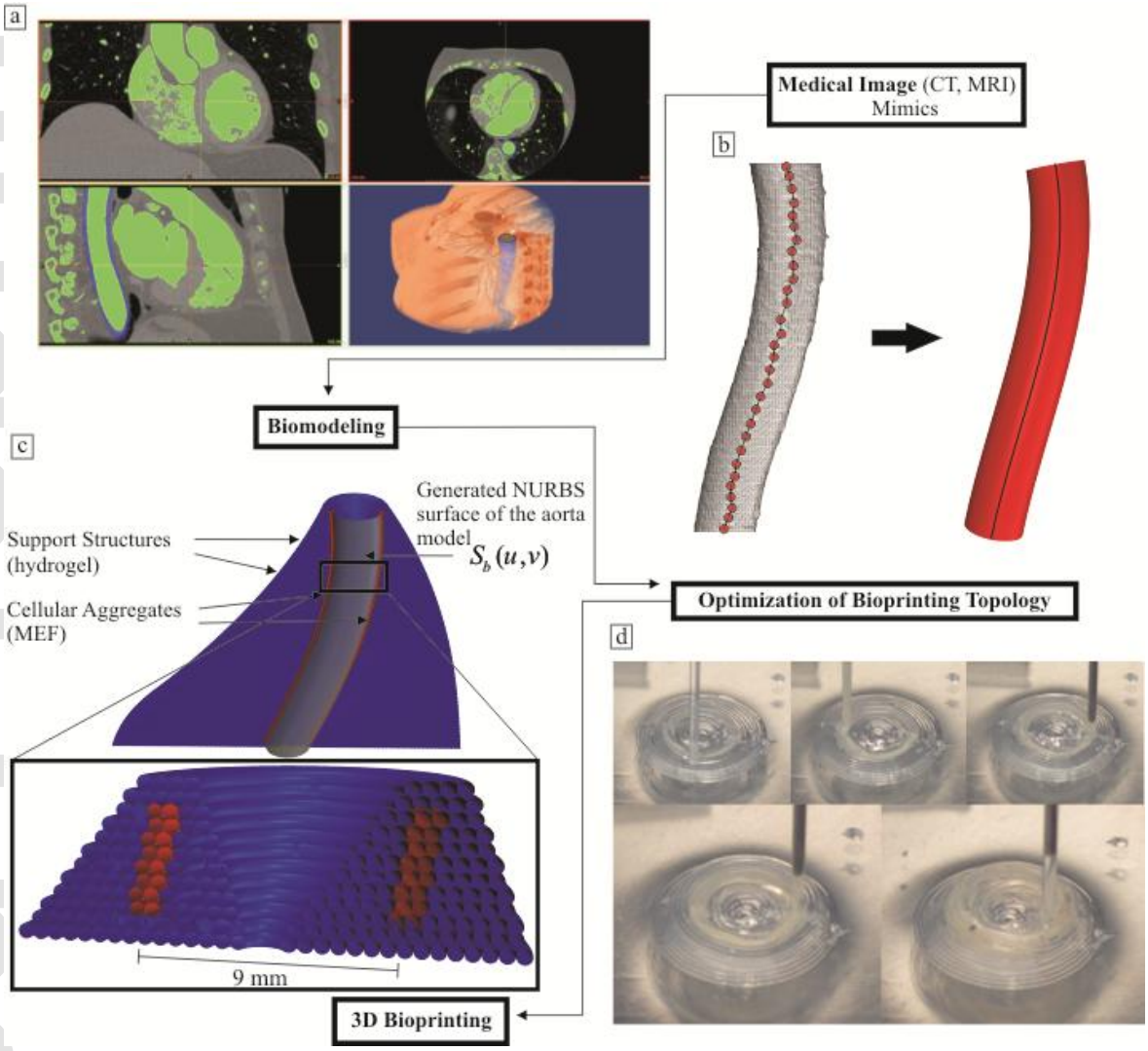

Figure 2

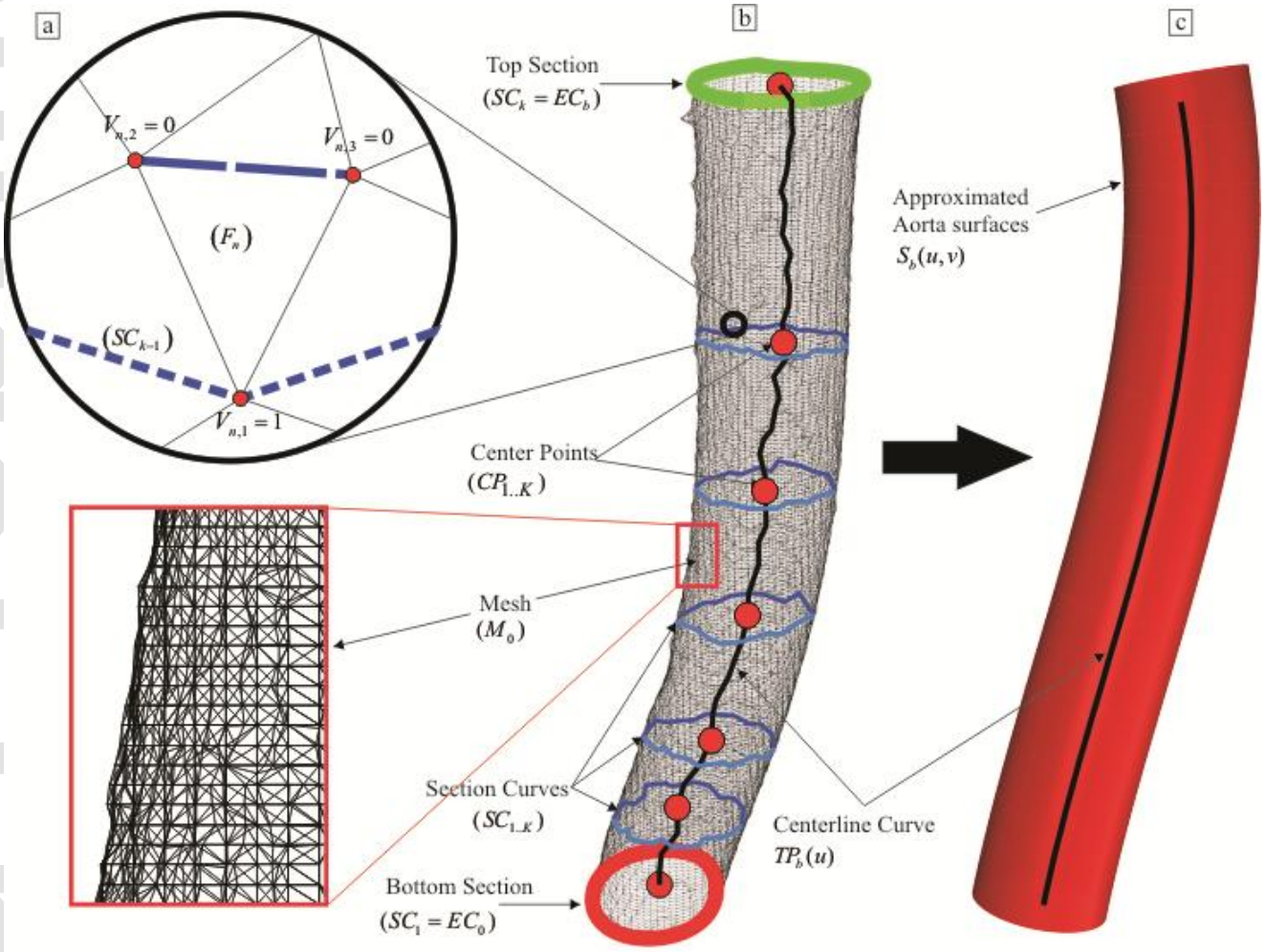

Figure 3

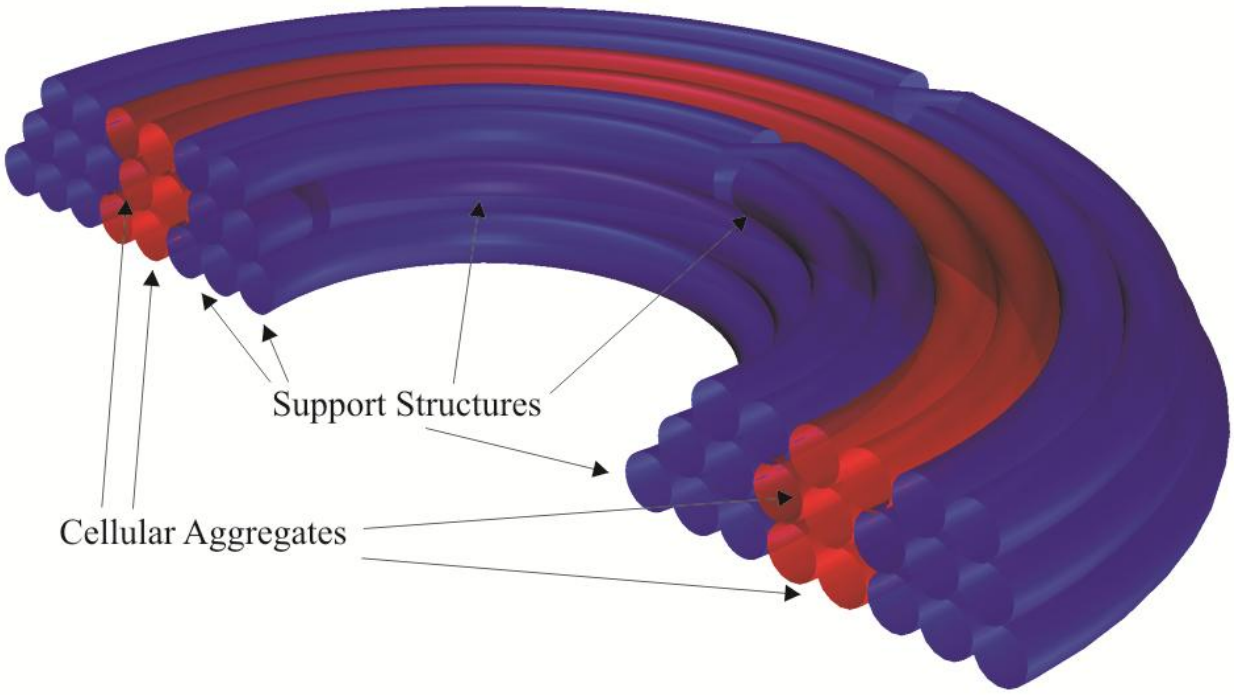

Figure 4

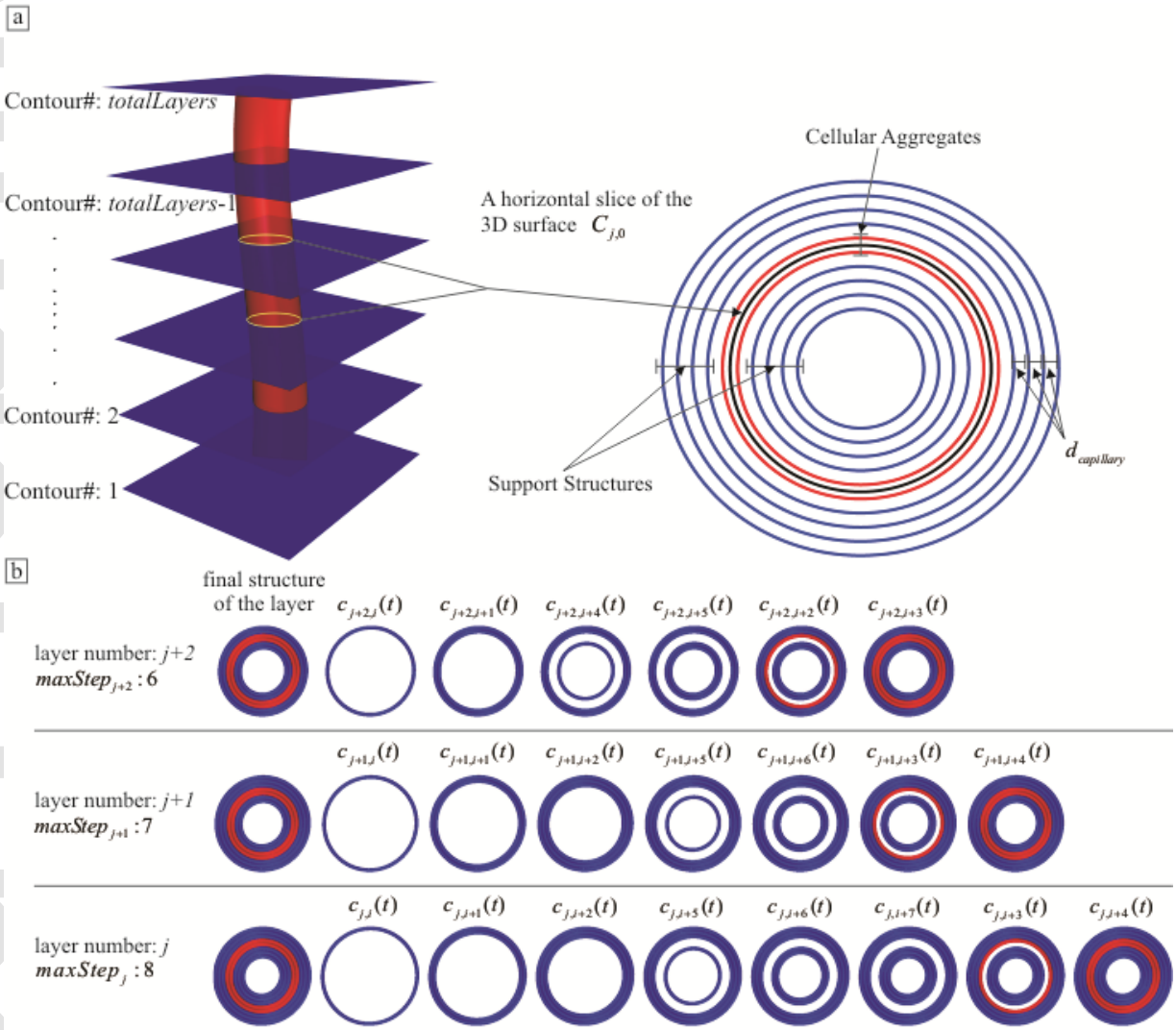

Figure 5

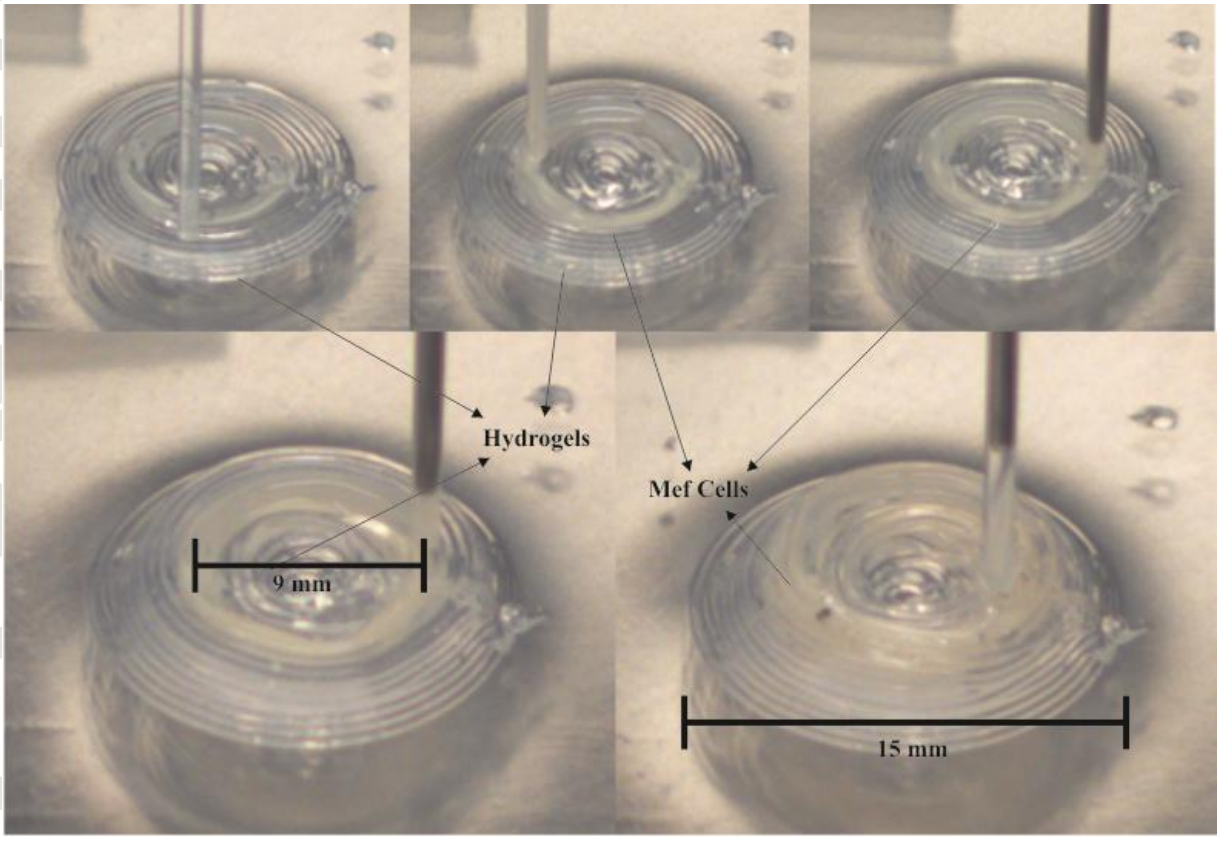

Figure 6

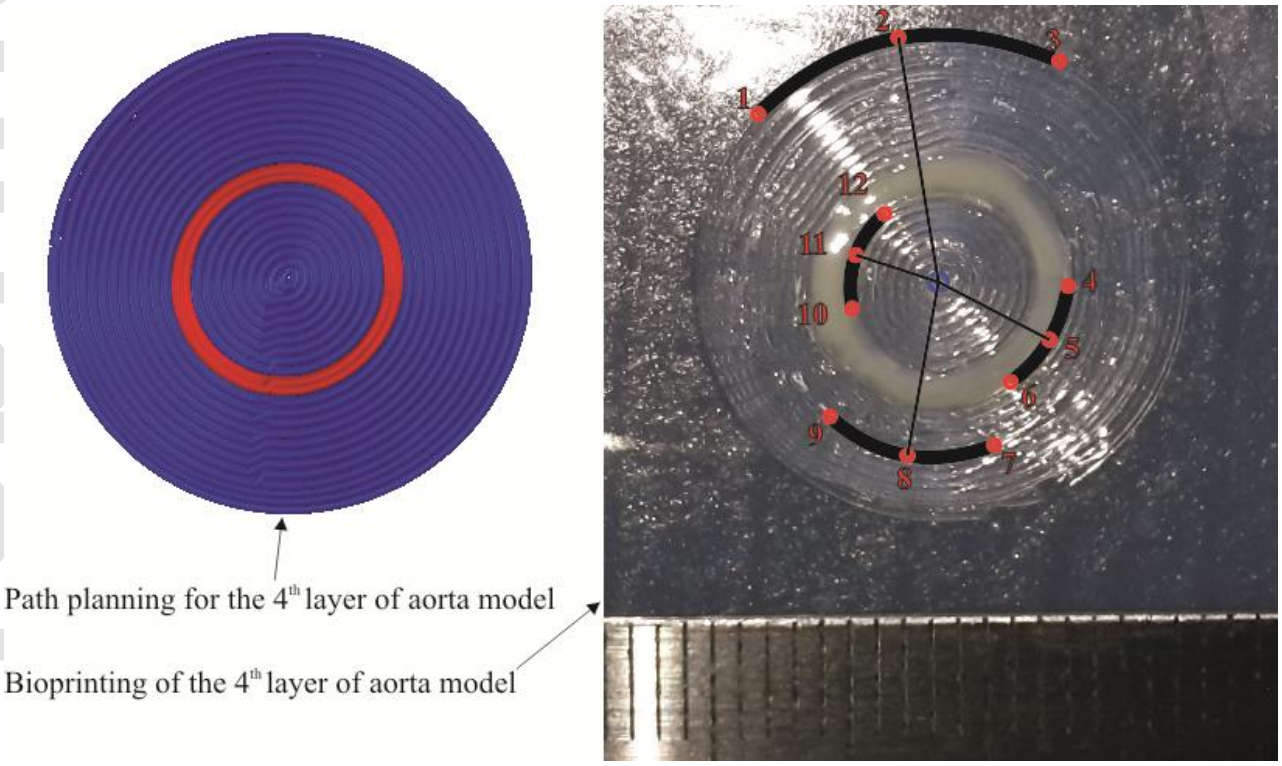

Figure 7

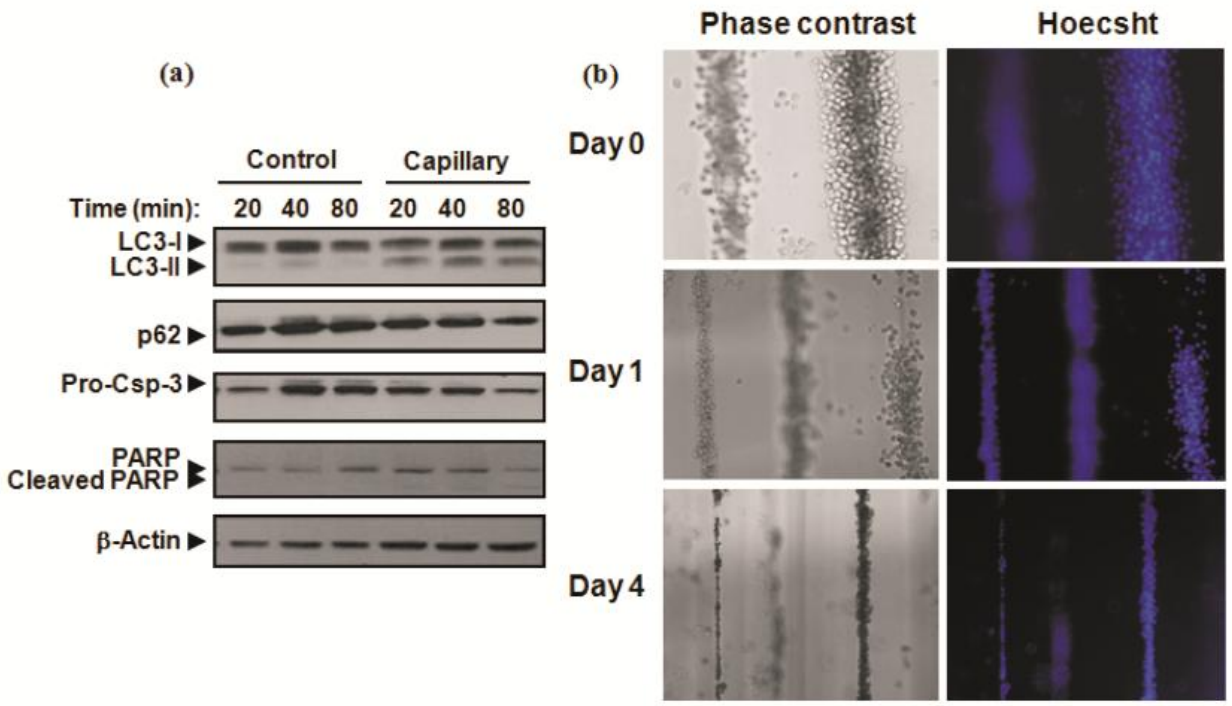

Figure 8

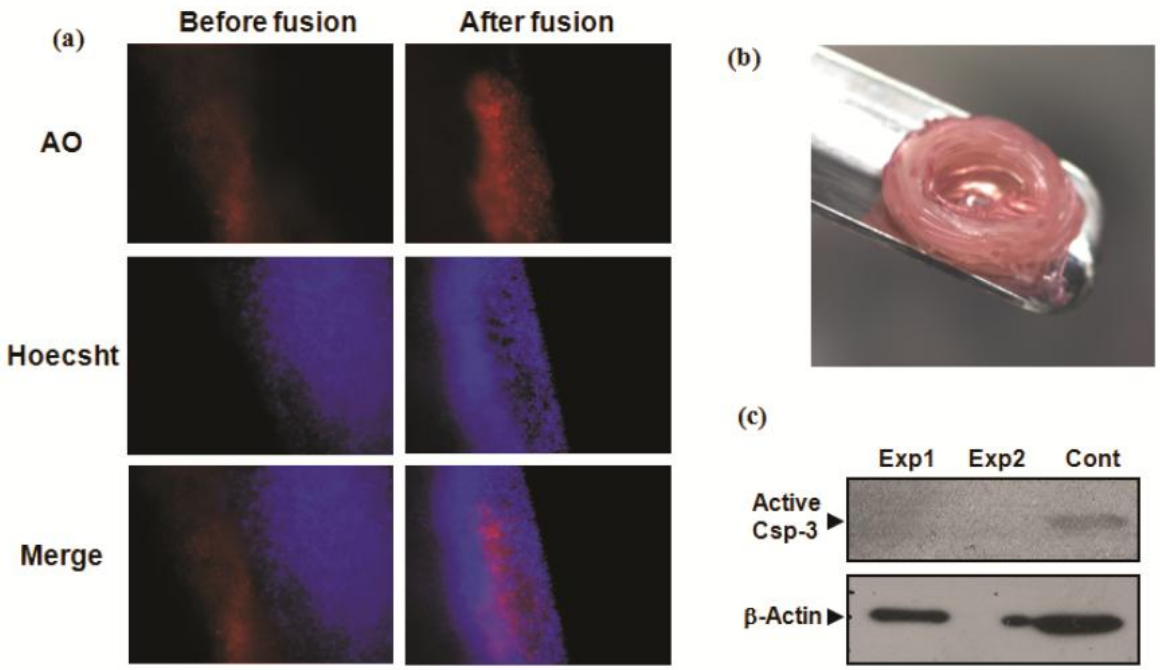

Figure 9